

ARTICLES

Production of Vibrationally Excited $\text{CN}(\text{B}^2\Sigma^+)$ via Superexcited Ion-Pair State of Triatomic Alkali-Metal Cyanides by $\text{Ar}(\text{}^3\text{P}_{2,0})$ ImpactHisato Yasumatsu,[†] Kaoru Suzuki,[‡] and Tamotsu Kondow^{*,†}

Department of Chemistry, School of Science, The University of Tokyo, Bunkyo-ku, Tokyo 113-0033, Japan

Received: February 25, 1998; In Final Form: May 28, 1998

Emission spectra from $\text{CN}(\text{B}^2\Sigma^+)$ produced by dissociative excitation of MCN ($\text{M} = \text{Rb}, \text{K}, \text{Na}$) in collision with $\text{Ar}(\text{}^3\text{P}_{2,0})$ were observed, and the mechanism of the energy partition between the two fragments was elucidated. The vibrational distribution of the $\text{CN}(\text{B}^2\Sigma^+)$ product is composed of two distinct components, P_L and P_H , ranged in the vibrational levels of $v' = 0-3$ and $11-19$, respectively, where v' is the vibrational quantum number of $\text{CN}(\text{B}^2\Sigma^+)$. The components, P_L and P_H , arise from direct dissociation and predissociation of MCN by $\text{Ar}(\text{}^3\text{P}_{2,0})$ impact, respectively. The direct dissociation proceeds on a repulsive potential energy surface correlating diabatically to $\text{M}(n\text{s}^2\text{S}) + \text{CN}(\text{B}^2\Sigma^+)$ ($n = 5, 4, 3$ for $\text{M} = \text{Rb}, \text{K}, \text{Na}$, respectively). This mechanism was further supported by a molecular dynamics simulation. The predissociation, on the other hand, proceeds via a superexcited ion-pair state, $\text{M}^+[\text{CN}^-]**$, having a much longer equilibrium C–N internuclear distance than that of $\text{CN}(\text{B}^2\Sigma^+)$, so that more than 90% of the excess energy is transmitted in the vibrational degree of freedom of the $\text{CN}(\text{B}^2\Sigma^+)$ product. In a framework of a state-crossing model, the extremely high vibrational excitation is explained by a large overlap between the vibrational wave functions of the superexcited $[\text{CN}^-]**$ and $\text{CN}(\text{B}^2\Sigma^+)$.

Introduction

Superexcited molecules, which have a larger internal energy than their electron binding energy, exhibit characteristic chemical and physical processes such as auto electron detachment, predissociation, and photoemission.^{1,2} Many experimental and theoretical studies have been extensively carried out mainly on superexcited covalent molecules. In this relation, we have investigated³ dissociation of triatomic molecules held by an ionic bond, such as an alkali-metal cyanide, MCN ($\text{M} = \text{K}, \text{Na}$),⁴ through covalent repulsive and ion-pair states. When MCN is excited to one of the superexcited states by collisional energy transfer from an argon metastable atom, $\text{Ar}(\text{}^3\text{P}_{2,0})$, the triatomic molecule is dissociated into $\text{M}(n\text{s}^2\text{S})$ and $\text{CN}(\text{B}^2\Sigma^+)$ as



where n is the principle quantum number of an alkali-metal atom ($n = 4$ and 3 for $\text{M} = \text{K}$ and Na , respectively). In the reaction of KCN , the $\text{CN}(\text{B}^2\Sigma^+)$ product is populated in two vibrational ranges, $v' = 0-3$ and $11-19$, where v' is the vibrational quantum number of $\text{CN}(\text{B}^2\Sigma^+)$. It has been concluded that superexcited repulsive and ion-pair states of KCN are responsible for the production of $\text{CN}(\text{B}^2\Sigma^+, v' = 0-3)$ and $\text{CN}(\text{B}^2\Sigma^+, v' = 11-19)$, respectively: (1) the direct dissociation pathway

on the potential energy surface of a superexcited repulsive state⁵ diabatically correlating to $\text{K}(4\text{s}^2\text{S}) + \text{CN}(\text{B}^2\Sigma^+)$ and (2) the predissociation pathway on the potential energy surface of the superexcited ion-pair state,⁵ $\text{K}^+[\text{CN}^-]**$, on which an adiabatic transition to the repulsive state leading to $\text{K}(4\text{s}^2\text{S}) + \text{CN}(\text{B}^2\Sigma^+)$ occurs at the crossing seam between the superexcited ion-pair state and the repulsive state. The superexcited ion-pair state of KCN has a much longer equilibrium C–N internuclear distance than that of $\text{CN}(\text{B}^2\Sigma^+)$,³ so that more than 90% of the available energy is transmitted to the vibrational degree of freedom of the $\text{CN}(\text{B}^2\Sigma^+)$ product. In the reaction of NaCN with $\text{Ar}(\text{}^3\text{P}_{2,0})$, on the other hand, $\text{CN}(\text{B}^2\Sigma^+, v' = 0-3)$ is observed,³ that is, only the direct dissociation proceeds. This characteristic feature is explained by energetics that the predissociative superexcited ion-pair state of NaCN lies in a higher energy range than the excitation energy of $\text{Ar}(\text{}^3\text{P}_{2,0})$.³

These findings indicate that the mechanism of the MCN dissociative excitation is controlled by the energetics of the superexcited states involved, which is changed greatly by changing M . The systematic study on the dissociative excitation of various MCN gives fundamental information on a chemical reaction via a superexcited ion-pair state. From this viewpoint, RbCN provides a unique opportunity to elucidate the reaction mechanism of MCN because its energetics is expected to admit both the direct dissociation and predissociation pathways in the collision with $\text{Ar}(\text{}^3\text{P}_{2,0})$. In the present study, the dissociative excitation of RbCN by the collisional energy transfer from $\text{Ar}(\text{}^3\text{P}_{2,0})$ was undertaken by measuring the vibrational and rotational distributions of the $\text{CN}(\text{B}^2\Sigma^+)$ product through observation of the $\text{CN}(\text{B}-\text{X})$ emission. The dissociation dynamics was

* To whom correspondence should be addressed.

[†] Present address: Cluster Research Laboratory, Toyota Technological Institute: in East Tokyo Laboratory, Genesis Research Institute, Inc., 717-86 Futamata, Ichikawa, Chiba 272-0001, Japan.[‡] Present address: Faculty of Foreign Studies, Tokoha Gakuen University, Sena, Shizuoka 420-0911, Japan.

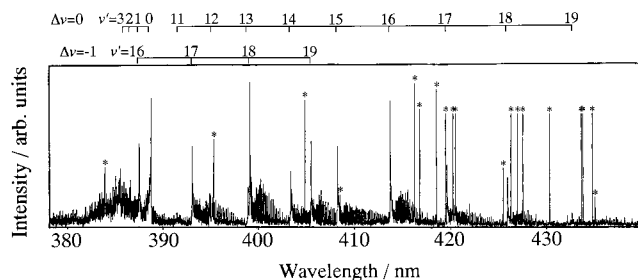


Figure 1. Typical emission spectrum of $\text{CN}(\text{B}^2\Sigma^+ - \text{X}^2\Sigma^+)$ $\Delta v = 0, -1$ sequences observed in the reaction of RbCN with $\text{Ar}(\text{P}_{2,0})$. In addition to the $\text{CN}(\text{B}^2\Sigma^+ - \text{X}^2\Sigma^+)$ emission, many resonant lines of Ar and Rb are observed (marked by *).

discussed in this reaction scheme, along with theoretical consideration by use of a molecular dynamics simulation³ and a state-crossing model.⁶

Experimental Section

A flowing afterglow method was used. As the experimental apparatus was the same as that used in the previous study,³ this paper gives only a brief description of the experimental procedure. An effusive molecular beam of RbCN was generated by vaporizing a RbCN crystalline sample in a tantalum crucible maintained at a temperature of 800 K. A vapor pressure of RbCN was estimated to be on the order of 1×10^{-1} Pa at this temperature, where the vapor pressure of RbCN is approximated by that of RbCl , as RbCN has similar physical properties to those of RbCl .^{5,7} The concentration of $(\text{RbCN})_2$ at this temperature is negligibly small.⁷ Argon metastable atoms were produced by microwave discharge of argon gas (99.9995% pure). Active species in the discharged Ar flow was $\text{Ar}^m(\text{P}_{2,0})$, and other active species did not take part in the present reaction.³ The concentration ratio, $[\text{Ar}(\text{P}_{2,0})]/[\text{Ar}(\text{P}_0)]$, was measured to be 11.³ Emission due to the $\text{CN}(\text{B}^2\Sigma^+ - \text{X}^2\Sigma^+)$ transition in the reaction region was dispersed by a monochromator (SPEX 1704), and detected by a single-photon counting method. The resolution of the spectra observed was 0.03 nm (fwhm) at a wavelength of 380 nm. The ambient pressure at the reaction region was maintained at 6×10^{-1} Pa. At this pressure, the collisional relaxation of the nascent vibrational and rotational distributions of the $\text{CN}(\text{B}^2\Sigma^+)$ product does not occur within the emission lifetime.⁸

The RbCN crystalline sample was synthesized by a neutralization reaction between rubidium hydroxide dissolved in anhydrous ethanol and hydrogen cyanide dissolved in anhydrous benzene under a dry argon atmosphere.⁹ An elemental analysis showed that the purity of the RbCN sample was more than 90% and that major impurities were the solvents used in the synthesis. To remove the solvents and water absorbed in the sample, the sample was heated to 400 K under an ambient pressure of 10^{-2} Pa for more than 10 h just before its use.

Results

Figure 1 shows $\Delta v = 0, -1$ sequences of the $\text{CN}(\text{B}^2\Sigma^+ - \text{X}^2\Sigma^+)$ emission spectrum observed in the reaction of RbCN with Ar^m . The emission spectrum consists of two components; one originates from $\text{CN}(\text{B}^2\Sigma^+, v' = 0-3)$ (P_L component) and the other from $\text{CN}(\text{B}^2\Sigma^+, v' = 11-19)$ (P_H component). With the $\text{CN}(\text{B}^2\Sigma^+ - \text{X}^2\Sigma^+)$ emission, many resonant lines of Ar and Rb are observed; the counterproducts of the excited Rb atoms could be $\text{CN}(\text{A}^2\Pi)$ and $\text{CN}(\text{X}^2\Sigma^+)$ by the energetics.

The vibrational and rotational distributions of the $\text{CN}(\text{B}^2\Sigma^+)$ product were obtained by the same simulation analysis as that

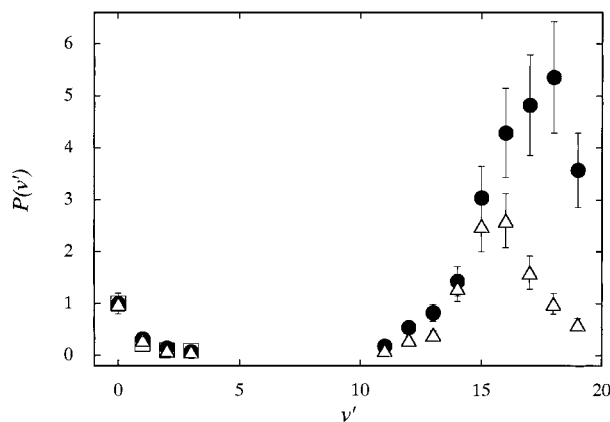


Figure 2. Vibrational population, $P(v')$, of $\text{CN}(\text{B}^2\Sigma^+, v')$ produced in the reactions of RbCN (●), KCN (△), and NaCN (□) with $\text{Ar}(\text{P}_{2,0})$ as a function of the vibrational quantum number, v' , of $\text{CN}(\text{B}^2\Sigma^+)$. The population at $v' = 0$, $P(0)$, is normalized to be unity.

used in the previous study.³ The rotational distribution of the $\text{CN}(\text{B}^2\Sigma^+)$ in each vibrational state was expressed well by a Boltzmann distribution with a rotational temperature in the range of 3000–600 K. The rotational temperatures thus obtained were the same as those obtained in the reaction of KCN (see Table 1 of ref 3).

Figure 2 shows the vibrational population, $P(v')$, of the $\text{CN}(\text{B}^2\Sigma^+)$ produced in the reaction of RbCN as well as those in the reactions of KCN and NaCN ,³ where the vibrational distribution is normalized to $P(0) = 1$. Uncertainties ($\sim 20\%$) in the vibrational populations originate mainly from an ambiguity in the simulation analysis.³ The vibrational distribution obtained from the P_L component (the P_L distribution) is independent of M , while that obtained from the P_H component (the P_H distribution) changes significantly from one MCN to another in the following manners: (1) the v' value for the maximum $P(v')$ in the P_H distribution is $v' = 18$ and 16 for the reactions of RbCN and KCN , respectively, and (2) the intensity ratio, $\sum_{v'=11}^{19} [\text{CN}(\text{B}^2\Sigma^+, v')]/\sum_{v'=0}^3 [\text{CN}(\text{B}^2\Sigma^+, v')]$, of the $\text{CN}(\text{B}^2\Sigma^+)$ product is 20, 8, and 0 for the reactions of RbCN , KCN , and NaCN , respectively.

The counter Rb atom of the $\text{CN}(\text{B}^2\Sigma^+, v' = 0-3)$ product is considered to be in the electronically ground state, $\text{Rb}(5s^2\text{S})$, as is the case of the NaCN reaction,³ because (1) the vibrational and rotational distributions of the $\text{CN}(\text{B}^2\Sigma^+, v' = 0-3)$ product in the reaction of RbCN are almost the same as those in the reaction of NaCN and (2) the excess energies for the reaction,



are almost the same as those for the reaction



where J' is the rotational quantum number of $\text{CN}(\text{B}^2\Sigma^+)$. On the other hand, the energetics allows only the counter atom, M , of $\text{CN}(\text{B}^2\Sigma^+, v' = 11-19)$ in its electronic ground state. Therefore, the energies available for the $\text{CN}(\text{B}^2\Sigma^+) + \text{Rb}(5s^2\text{S})$ products are 3.7 ± 0.2 and 3.9 ± 0.2 eV for the reaction of RbCN with $\text{Ar}(\text{P}_2)$ and $\text{Ar}(\text{P}_0)$, respectively.¹⁰ They are almost the same as those for the reactions of NaCN and KCN .³

Discussion

As described in the previous section, the vibrational distribution of the $\text{CN}(\text{B}^2\Sigma^+)$ produced in the reaction of RbCN with Ar^m consists of the two distinct components, P_L and P_H

distributions, as observed in the KCN reaction.³ The P_L and P_H distributions for the RbCN reaction are almost identical to those of KCN.³ These results lead us to conclude that the same mechanism operates in the dissociative excitation of RbCN and KCN, i.e., $\text{CN}(\text{B}^2\Sigma^+, v' = 0-3)$ and $\text{CN}(\text{B}^2\Sigma^+, v' = 11-19)$ are produced by the direct dissociation and the predissociation via superexcited states, respectively.³ In the following subsections, the dynamics of the direct dissociation and the predissociation via the superexcited states are discussed separately and the roles of the counter atom, M, are clarified.

Direct Dissociation for $\text{CN}(\text{B}^2\Sigma^+, v' = 0-3)$ Production.

The direct dissociation of MCN proceeds on a repulsive potential energy surface³ which correlates diabatically to $\text{M}(ns^2 \text{S}) + \text{CN}(\text{B}^2\Sigma^+)$ ($n = 3, 4, \text{ and } 5$ for $\text{M} = \text{Na}, \text{K}$ and Rb) after the Franck–Condon excitation of MCN by the energy transfer from Ar^m . In this channel, more than 90% of the available energy is transmitted to the translational energies of $\text{M}(ns^2 \text{S})$ and $\text{CN}(\text{B}^2\Sigma^+)$, and a small portion of the available energy is shared by the vibrational and rotational modes of $\text{CN}(\text{B}^2\Sigma^+)$. The nearly exclusive energy transmission to the translational degree of freedom is explained by the fact that the dissociation in the repulsive state starts from the T-shape geometry due to the Franck–Condon excitation from the T-shaped ground state¹⁴⁻¹⁷ to the repulsive state. The recoil between M and $\text{CN}(\text{B}^2\Sigma^+)$ starting from the T-shape geometry does not result in the rotational and vibrational excitation of the $\text{CN}(\text{B}^2\Sigma^+)$ product because the dissociation coordinate between M and CN is orthogonal to the M–CN locking and the C–N stretching vibrational modes of MCN, which directly couple with the rotation and the vibration of the $\text{CN}(\text{B}^2\Sigma^+)$ product, respectively. Instead, the M and $\text{CN}(\text{B}^2\Sigma^+)$ products gain a translational energy as large as ~ 3.5 eV. Furthermore, the adiabatic transition probability from the repulsive state to another state is considered to be very small, although the repulsive state crosses with many other excited states, e.g., superexcited ion-pair states.⁵

The mass effect on the direct dissociation pathway was further examined by a molecular dynamics simulation. The vibrational and rotational distributions of the $\text{CN}(\text{B}^2\Sigma^+)$ product were calculated by solving the equations of motion with an algorithm of the Verlet method.¹⁸ The method of the calculation is almost the same as that employed in the previous study,³ except for including the thermal distribution of the initial C–N internuclear distance of the parent MCN. The distribution function of the initial C–N distance was approximated by a square of the wave function of a harmonic oscillator having the vibrational frequency equal to that of the C–N stretching of MCN (2163.9 cm^{-1}).¹⁹ It is sufficient to take into account only the ground state of the C–N stretching vibration because the C–N stretching vibration of the parent MCN has a population in the ground state at the oven temperature of 800 K; the energy of the C–N stretching vibration ($\sim 0.25 \text{ eV}$ ¹⁹) is much larger than the thermal energy of the parent MCN ($1/2 k_B T = 0.04 \text{ eV}$ for $T = 800 \text{ K}$). The distribution of the initial M–C–N bending angle was assumed to obey the Boltzmann distribution at the oven temperature, where the potential energy surfaces along the M–C–N bending coordinate were obtained from refs 16 and 17.

The intramolecular potential energy of MCN in the repulsive state (excited state) was constructed by a sum of diatomic pair potentials of the M–C, M–N, and C–N pairs; the diatomic potentials between C and N were approximated by a harmonic oscillator potential having the same frequency as that of $\text{CN}(\text{B}^2\Sigma^+)$ ¹³ and that between M and Y ($Y = \text{C}$ and N) were

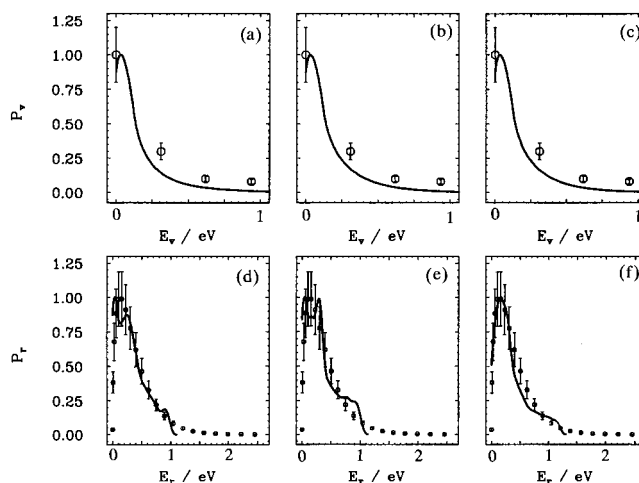


Figure 3. Calculated vibrational and rotational distributions (solid curves), P_v and P_r , respectively, of the direct dissociation product, $\text{CN}(\text{B}^2\Sigma^+, v' = 0-3)$, by use of the molecular dynamics simulation (see text), along with the experimental ones (\circ). The vibrational distributions in the reactions of NaCN, KCN, and RbCN are shown in panels a, b, and c, respectively, and the rotational distributions in the reactions of NaCN, KCN, and RbCN are in panels d, e, and f, respectively. The energies, E_v and E_r , are the vibrational and rotational energies of $\text{CN}(\text{B}^2\Sigma^+)$, respectively, where the zero-point vibrational energy of $\text{CN}(\text{B}^2\Sigma^+)$ ($= 0.125 \text{ eV}$) is subtracted from E_v .

by soft core potentials, $\alpha_{\text{MY}} r_{\text{MY}}^{-n, 20}$ where r_{MY} denotes the internuclear distance between M and Y. The two values, $\alpha = \alpha_{\text{MC}}/\alpha_{\text{MN}}$ and n , were used as adjustable fitting parameters. The vibrational and rotational distributions of the $\text{CN}(\text{B}^2\Sigma^+)$ product were obtained by averaging the trajectory runs starting from more than 5000 different initial geometries in the Boltzmann distribution at the oven temperature. The time step and the duration for the integration of the equations of motion were 0.1 and 40 fs, respectively, which were found to be sufficient in the direct dissociation pathway.

Figure 3 shows the calculated vibrational and rotational distributions of the $\text{CN}(\text{B}^2\Sigma^+)$ product as functions of the vibrational and rotational energies, respectively; the best-fit parameters used for these calculations are $(n, \alpha) = (7.0, 3.0)$, $(6.5, 2.5)$, and $(7.0, 2.5)$ for NaCN, KCN, and RbCN, respectively. The calculated results well reproduce the experimental ones, and the values of the best-fit parameters are almost identical for the three MCN. These results support that the $\text{CN}(\text{B}^2\Sigma^+)$ is produced by the direct dissociation in a repulsive state correlating diabatically to $\text{M}(^2\text{S}) + \text{CN}(\text{B}^2\Sigma^+)$; the potential energy surface of the repulsive state is as steep as r_{MY}^{-7} along the dissociation coordinate. The shape of the potential energy surface described by the best-fit parameters is almost the same as that of the repulsive states of alkali-metal halogen diatomic molecules.²⁰

Predissociation for $\text{CN}(\text{B}^2\Sigma^+, v' = 11-19)$ Production.

The mean value of the vibrational energy of the $\text{CN}(\text{B}^2\Sigma^+, v' = 11-19)$ product is as high as 90% of the available energy for the $\text{CN}(\text{B}^2\Sigma^+)$ product. This exclusive energy transmission to the vibrational degree of freedom of the $\text{CN}(\text{B}^2\Sigma^+)$ product originates from the predissociation of MCN via a superexcited state having an equilibrium C–N internuclear distance, r_{CN}^e , much longer than that of $\text{CN}(\text{B}^2\Sigma^+)$ ($r_{\text{CN(B)}}^e = 1.15 \text{ \AA}$ ¹³). As electronically excited states of CN^- , $[\text{CN}^-]**$, were found to have a very long r_{CN}^e (typically 1.4 \AA for $\text{CN}^-(^3\Sigma^+)$) by our ab initio calculation (see below), the predissociative excited state for the production of $\text{CN}(\text{B}^2\Sigma^+, v' = 11-19)$ is likely to be a superexcited ion-pair state, $\text{M}^+[\text{CN}^-]**$. First of all, MCN is

excited to the superexcited ion-pair state, $M^+ \cdot [CN^-]**$, by the energy transfer from Ar^m , and the internuclear distance of the CN moiety is elongated. Then, adiabatic transition occurs from the superexcited ion-pair state to a repulsive state diabatically correlating to $M(ns^2S) + CN(B^2\Sigma^+, v' = 11-19)$, and finally, $CN(B^2\Sigma^+, v' = 11-19)$ is produced. The electronic excited state of CN^- lies in the energy range higher than the electron binding energy of CN^- (3.821 eV¹³), so that the adiabatic transition from $M^+ \cdot [CN^-]**$ to the final repulsive state is regarded as electron transfer from $[CN^-]**$ to M^+ .

As shown in Figure 2, the $CN(B^2\Sigma^+, v' = 11-19)$ produced in the reaction of $RbCN$ is vibrationally excited to a higher extent than that produced in the reaction of KCN , whereas no $CN(B^2\Sigma^+, v' = 11-19)$ is produced in the reaction of $NaCN$. To clarify the role of M in the predissociation of MCN , a state-crossing model⁶ was applied to calculate the vibrational distribution of the predissociation product, $CN(B^2\Sigma^+, v' = 11-19)$. Here, it is assumed that the C–N stretching vibration does not couple with neither the M–CN stretching nor M–C–N bending motions because these motions are almost orthogonal to the C–N stretching vibration in the T-shape geometry of MCN .¹⁴⁻¹⁷ Actually, the bending motion of MCN is not much excited because the rotational temperatures of the $CN(B^2\Sigma^+, v' = 11-19)$ products are comparable to that of the parent molecule, MCN (see Table 1 of ref 3). For simplicity, let us consider a single superexcited ion-pair state involved in the predissociation channel. Then, the vibrational population, $P(v')$, of the $CN(B^2\Sigma^+, v' = 11-19)$ product is given by the summation of a product between (1) a Franck–Condon factor between the C–N stretching vibration of MCN in the ground and in predissociative superexcited ion-pair states and (2) an adiabatic transition probability from the superexcited ion-pair state to the final repulsive state

$$P(v') \propto \sum_{v^g, v^e} \{ |\langle v^g | v^e \rangle|^2 Q(v^e \rightarrow v') \} \quad (4)$$

where v^g and v^e are the quantum numbers of the C–N stretching vibration of MCN in the ground and superexcited ion-pair states, respectively, $|v\rangle$ is a vibrational wave function associated with the v 'th level of the C–N stretching vibration, and $Q(v^e \rightarrow v')$ is the adiabatic transition probability from the superexcited ion-pair state, $M^+ \cdot [CN^-(v^e)]**$, to the final repulsive state, $M(^2S) \cdot CN(B^2\Sigma^+, v')$. The first term, $|\langle v^g | v^e \rangle|^2$, of eq 4 is the Franck–Condon factor between the C–N stretching vibration of MCN in the ground and in the superexcited ion-pair states. The summation in eq 4 is calculated in the v^e range energetically accessible by the Ar^m excitation. It is sufficient to take only $v^g = 0$ into consideration because the C–N stretching vibration of the parent MCN molecule populates only in the vibrational ground state at the present oven temperature as stated in the previous subsection.

The adiabatic transition probability, $Q(v^e \rightarrow v')$, is given^{6,21} by

$$Q(v^e \rightarrow v') = 1 - \exp \left(- \frac{\sqrt{2\pi} |\langle v^e | v' \rangle|^2 \alpha^2}{\sqrt{f_1 - f_2} \sqrt{\epsilon(f_1 - f_2) + \sqrt{4\alpha^2 f^2 + \epsilon^2 (f_1 - f_2)^2}}} \right) \quad (5)$$

where α is a matrix element of nonadiabatic interaction between the superexcited ion-pair state and the final repulsive state, ϵ is a relative translational energy between M^+ and $[CN^-]**$ when the $M^+ + [CN^-]**$ system passes through the potential crossing

seam between the superexcited ion-pair state and the final repulsive state, f_1 and f_2 are the gradients of the potential energy curves of the superexcited ion-pair state and the final repulsive state, respectively, along the dissociation coordinate, and $f = (f_1 |f_2|)^{1/2}$. The term, $|\langle v^e | v' \rangle|^2$, is the Franck–Condon factor between the C–N stretching vibration of MCN in the superexcited ion-pair state and in the final repulsive state.

As the M–CN distance at the crossing seam is longer than 2.5 Å, the potential energies, V_1 and V_2 , of the superexcited ion-pair state and the final repulsive state are well mimicked by a Coulomb attractive potential^{20,23} and a constant potential, respectively

$$V_1 = -(1/R_{M-CN}) + E^{IP}(v^e) \quad (6)$$

and

$$V_2 = E^B(v') \quad (7)$$

where R_{M-CN} is the distance between M and CN , and $E^{IP}(v^e)$ and $E^B(v')$ are the potential energies of the superexcited ion-pair state and the final repulsive state at the corresponding dissociation limits, $M^+ + [CN^-(v^e)]**$ and $M(^2S) + CN(B^2\Sigma^+, v')$, respectively, with respect to the potential energy of the ground state of MCN . These potential energies at the dissociation limits are calculated by

$$E^{IP}(v^e) = D(M-CN) + I_E(M) - EA(CN) + E_1(v^e) \quad (8)$$

and

$$E^B(v') = D(M-CN) + E_2(v') \quad (9)$$

respectively, where $D(M-CN)$, $I_E(M)$, $EA(CN)$, $E_1(v^e)$, and $E_2(v')$ are the bond dissociation energy of MCN into $M(^2S) + CN(X^2\Sigma^+)$,¹² the ionization energy of M , the electron affinity of CN (3.821 eV²⁴), and the sums of the electronic and vibrational energies of $[CN^-(v^e)]**$ and $CN(B^2\Sigma^+, v')$, respectively. The electronic matrix element, α , is calculated from V_1 and V_2 by using Olson's method.²³

The C–N stretching wave functions, $|v^e\rangle$ and $|v'\rangle$, of the superexcited ion-pair state and the final repulsive state were approximated by those of a bare $[CN^-]**$ and $CN(B^2\Sigma^+)$, respectively, where the latter was obtained from the RKR potential of $CN(B^2\Sigma^+)$ ²² and the former by an ab initio calculation. In the ab initio calculation, the multireference (MR) configuration interaction (CI) method was used. The basis set used for the C and N atoms is [521/211/1] derived from (53/4) in Huzinaga's book,²⁵ complemented with a diffuse p-type function. In the generation of the reference electron configurations for CI, all valence molecular orbitals (MO) are included in the active orbital space and, in addition four diffuse MOs are added to them. The superexcited states of CN^- are described under a restriction that one electron always occupies one of the diffuse MOs. By this method, the lowest energy states having symmetries of $^1\Sigma^+$, $^1\Sigma^-$, $^1\Pi$, $^1\Delta$, $^3\Sigma^+$, $^3\Sigma^-$, $^3\Pi$, and $^3\Delta$ were obtained. The internuclear distances, r_{CN}^e , of these states are elongated because of one or more electrons in antibonding molecular orbitals such as $(2\pi)^*$ and $(6\sigma)^*$. A potential energy curve of one of these excited states was used as that of $[CN^-]**$ in the calculation, along with the electronic energy of $[CN^-]**$ used as an adjustable fitting parameter, $E_1(v^e = 0)$, (see eq 8) so as to reproduce the experimental vibrational distribution of the $CN(B^2\Sigma^+, v' = 11-19)$ product.

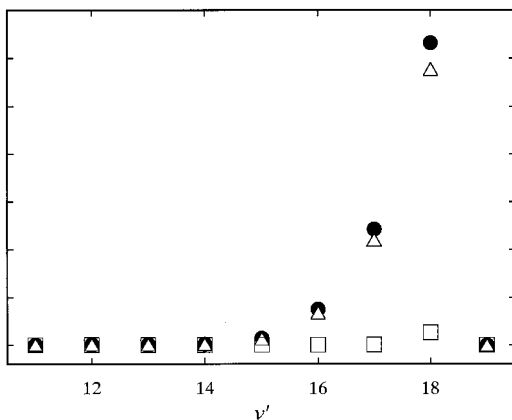


Figure 4. Calculated vibrational population, $P(v')$, of $\text{CN}(\text{B}^2\Sigma^+, v' = 11-19)$, produced in the reactions of RbCN (\bullet), KCN (Δ) and NaCN (\square) as a function of the vibrational quantum number, v' , of $\text{CN}(\text{B}^2\Sigma^+)$. The calculation was performed by use of the state-crossing model (see the text).

Figure 4 shows the best-fit vibrational populations, $P(v')$, of the $\text{CN}(\text{B}^2\Sigma^+, v' = 11-19)$ product calculated with the potential energy curve of the $\text{CN}^-(1^3\Sigma^-)$ state and its electronic energy of $E_1(v^e = 0) = 11.0$ eV.²⁶ The shape of the vibrational distribution of the $\text{CN}(\text{B}^2\Sigma^+, v' = 11-19)$ product is almost the same as that calculated (see Figure 2). The high vibrational excitation originates from the large vibrational overlap, $|\langle v^e | v' \rangle|^2$, in the $v' = 16-18$ range. The calculation shows, as well, that no production of $\text{CN}(\text{B}^2\Sigma^+, v' = 11-19)$ in the reaction of NaCN arises from the energetics that the superexcited ion-pair state of NaCN is not accessible by the Ar^m excitation. The intensity ratio, $\sum_{v'=11}^{19} [\text{CN}(\text{B}^2\Sigma^+, v')] / \sum_{v'=0}^3 [\text{CN}(\text{B}^2\Sigma^+, v')]$, in the reaction of RbCN is larger than that in the reaction of KCN because of the larger $Q(v^e \rightarrow v')$ in the reaction of RbCN than that in KCN .

Acknowledgment. The authors are grateful to Professor Suehiro Iwata for his help and discussion on the ab initio calculations of CN^- . We also appreciate Professor Haruhiko Ito for providing us the RKR potential energy curve of $\text{CN}(\text{B}^2\Sigma^+)$. This research was supported by the Special Cluster Research Project of Genesis Research Institute, Inc. and Grant-in-Aid for General Scientific Research from the Ministry of Education, Science and Culture.

References and Notes

- (1) Illenberger, E.; Momigny, J. *Gaseous Molecular Ions. An Introduction to Elementary Processes Induced by Ionization*; Springer-Verlag: New York, 1992.
- (2) Hatano, Y. In *Dynamics of excited molecules*; Kuchitsu, K., Ed.; Elsevier: Amsterdam, 1994; Chapter 6.
- (3) Yasumatsu, H.; Suzuki, K.; Kondow, T. *J. Phys. Chem.* **1993**, *97*, 6788.
- (4) Bowling, R. A.; Allen, J. D., Jr.; Schweitzer, G. K. *J. Electron Spectrosc. Relat. Phenom.* **1979**, *16*, 489.
- (5) Yasumatsu, H.; Kondow, T.; Suzuki, K.; Tabayashi, K.; Shobatake, K. *J. Phys. Chem.* **1994**, *98*, 1407.
- (6) Bauer, E.; Fisher, E. R.; Gilmore, F. R. *J. Chem. Phys.* **1969**, *51*, 4173.
- (7) Knache, O.; Kubaschewski, O.; Hesselmann, K. *Thermochemical Properties of Inorganic Substances*; Springer-Verlag: New York, 1991; 1655.
- (8) Kanda, K.; Ito, H.; Someda, K.; Suzuki, K.; Kondow, T.; Kuchitsu, K. *J. Phys. Chem.* **1989**, *93*, 6020.
- (9) DeLong, M. C.; Rosenbeger, F. *J. Cryst. Growth* **1986**, *75*, 164.
- (10) The excess energies are calculated from the excitation energies of $\text{Ar}(^3\text{P}_{2,0})$,¹¹ the bond dissociation energy of RbCN into $\text{Rb}(^2\text{S}) + \text{CN}(X^2\Sigma^+)$,¹² and the electronic excitation energy of $\text{CN}(\text{B}^2\Sigma^+)$.¹³
- (11) Setser, D. W. *Reactive Intermediates in the Gas Phase*; Academic Press: New York, 1979; Chapter 3.
- (12) L'vov, B. V.; Pelieva, L. A. *Prog. Anal. Atom. Spectrosc.* **1980**, *3*, 65.
- (13) Huber, H.; Herzberg, G. *Molecular Spectra and Molecular Structure IV. Constants of Diatomic Molecules*; Van Nostrand Reinhold: New York, 1979.
- (14) van Vaals, J. J.; Meerts, W. L.; Dymanus, A. *Chem. Phys.* **1984**, *86*, 147.
- (15) van Vaals, J. J.; Meerts, W. L.; Dymanus, A. *J. Mol. Spectrosc.* **1984**, *106*, 280.
- (16) Marsden, C. J. *J. Chem. Phys.* **1982**, *76*, 6451.
- (17) Leuken, E.; Brocks, G.; Wormer, P. E. S. *Chem. Phys.* **1986**, *110*, 365.
- (18) Verlet, L. *Phys. Rev.* **1967**, *159*, 98.
- (19) Ismail, Z. K.; Hauge, R. H.; Margrave, J. L. *J. Mol. Spectrosc.* **1975**, *54*, 402.
- (20) Zeiri, Y.; Balint-Kurti, G. G. *J. Mol. Spectrosc.* **1983**, *99*, 1.
- (21) Zhu, C.; Nakamura, H. *J. Chem. Phys.* **1993**, *98*, 6208.
- (22) Ito, H. Private communication.
- (23) Olson, R. E.; Smith, F. T.; Bauer, E. *Appl. Opt.* **1971**, *10*, 1848.
- (24) Klein, R.; McGinnis, R. P.; Leone, S. R. *Chem. Phys. Lett.* **1983**, *100*, 1475.
- (25) Huzinaga, S. *Gaussian Basis Sets for Molecular Calculations*; Elsevier: Amsterdam, 1984.
- (26) The electronic energy of the first $\text{CN}^-(^3\Sigma^-)$ state was calculated to be 5.5 eV by the ab initio method, while the best-fit parameter, $E_1(v^e = 0)$, is 11.0 eV. Thus, the first $\text{CN}^-(^3\Sigma^-)$ state would not be involved in the superexcited ion-pair state contributing to the predissociation.